Routes to chaos in the balanced two-photon Dicke model with qubit dissipation

Jiahui Li[1,2] and Stefano Chesi[2,3,*]

[1]*School of Future Technology, Henan University, Zhengzhou 450046, China*
[2]*Beijing Computational Science Research Center, Beijing 100193, China*
[3]*Department of Physics, Beijing Normal University, Beijing 100875, China*

(Received 18 August 2023; accepted 20 March 2024; published 1 May 2024)

We study the semiclassical limit of the two-photon Dicke model with both cavity decay and qubit dissipation, and extend a recent analysis of its stationary points [Garbe *et al.*, Sci. Rep. **10**, 13408 (2020)], where a large unstable region was found. By considering the explicit dynamical evolution, we show that the unstable region actually hosts a rich nonlinear behavior. At variance with other types of Dicke models (without qubit dissipation or with one-photon interactions), the occurrence of chaos does not rely on a large counterrotating interaction. Furthermore, new routes to chaos appear in addition to period-doubling bifurcations, i.e., intermittent chaos and quasi-periodic oscillations. The transition mechanisms under these three distinct routes are investigated in detail through the system's long-time evolution, the optical field power spectrum, Lyapunov exponents, and bifurcation diagrams. Additionally, we provide a comprehensive phase diagram detailing the existence of stable fixed points, limit cycles, and the aforementioned chaos-related dynamics.

DOI: 10.1103/PhysRevA.109.053702

I. INTRODUCTION

Chaos, famous for its "butterfly effect," is one of the most vital subjects in nonlinear science, with significant applications in the fields of secure communication and encryption [1,2]. It is particularly relevant for quantum optical systems where, benefiting from the rapid development of integrated quantum technology, chaotic dynamics has been investigated in a variety of platforms, such as optomechanics [3–7], nonlinear magnonics [8–11], and Dicke-type models [12–15]. However, most of such realizations can only access specific types of nonlinear behaviors. An important example concerns the transition from a steady state to chaos, which occurs via various periodic and quasi-periodic states and is commonly referred to as "route to chaos." Chaos can appear following a "period-doubling" route, where a cascade of pitchfork bifurcations leads to oscillatory dynamics with period T, $2T$, $4T$, ..., until the chaotic dynamics is finally established. This behavior has been typically observed in various types of Dicke models [16–18] and in optomechanics [4]. However, other routes to chaos exist in general [1,2]. We show here that the two-photon Dicke model *with qubit dissipation* can support several distinct routes to chaos, depending on the system's parameters.

The quantum Dicke model has sparked profound research in the past decades [12,13]. It describes a collective interaction between N qubits and a single bosonic mode which, in the strong coupling regime, can induce many interesting equilibrium and nonequilibrium phenomena, such as a superradiant phase (SP) transition [19–28], multistability [29,30], and classical and quantum chaos [31–35]. The implementation of this model with analog quantum simulators makes it possible to examine these phenomena in several experimental platforms [36,37], such as trapped ions [38,39], arrays of nitrogen-vacancy (NV) centers [40], and superconducting circuits [41–43]. In these driven-dissipative systems, multiphoton processes can be selected from linear interactions by properly adjusting the driving lasers' parameters. Therefore, an interesting variation of the Dicke model considering a two-photon interaction has received much interest recently, and has been shown to display a variety of intriguing dynamical behaviors [14,15,18,44–50].

For the closed one-photon Dicke model, a transition from quasi-integrability to quantum chaos is predicted to occur after the superradiant phase transition has taken place [51–54]. Accounting for dissipation, the observation of classical chaos has been only reported so far in models with an unbalanced interaction, i.e., where the coupling strength of the counterrotating terms is larger than the corotating terms [16–18]. The study of classical nonlinear dynamics arises naturally in Dicke-type models, since the semiclassical limit becomes exact at large N [55–57]. Taking cavity loss into consideration, Refs. [16] and [18] analyzed the one- and two-photon Dicke models, respectively, finding a rich dynamical behavior including Hopf bifurcations, period doubling, and strange attractors. However, these studies assumed that the dominant decoherence mechanism is from the bosonic field, while neglecting qubit dissipation.

In this paper we extend the above study of the two-photon Dicke model [18] by including the influence of atomic dissipation. We find that this effect has a profound influence on the system properties, leading to qualitative changes in the nonlinear behavior: qubit dissipation not only benefits system stability, but also results in a richer scenario for the occurrence of chaotic dynamics. Differently than models without qubit decoherence [16,18], additional routes to chaos are available here (besides period-doubling bifurcations). We list them in

*stefano.chesi@csrc.ac.cn

TABLE I. Representative examples of chaotic dynamics in various types of Dicke models. The first column differentiates between one- and two-photon interactions (1ph and 2ph, respectively). The second column indicates the dissipation channels. Note that $\Gamma_\uparrow$ (second line) refers to incoherent pumping. λ is the ratio between counter- and corotating couplings. Detailed parameters are as indicated by the last column. Their values are generally similar to the ones used in this work.

Model	Dissipation	Anisotropy	Route to chaos	Reference
1ph	κ	$\lambda \gtrsim 1.75$	Period doubling, global bifurcation	Fig. 16 of Ref. [16] ($\lambda_- = 1$)
1ph	$\kappa, \Gamma_\downarrow, \Gamma_\uparrow$	$\lambda \simeq 2.3$	Period doubling	Fig. 9 of Ref. [17]
2ph	κ	$\lambda \simeq 2.15$	Period doubling	Fig. 8(a) of Ref. [18]
2ph	$\kappa, \Gamma_\downarrow, \Gamma_\phi$	$\lambda = 1$	Period doubling, intermittency, quasi-periodicity	This work

the fourth column of Table I, which presents a comparison of several instances of chaos in Dicke-type models. One can also appreciate from Table I that in this case the chaotic dynamics survives in the isotropic limit ($\lambda = 1$), thus does not rely on strong counterrotating terms.

We finally comment about the relationship of our study with the stability of the model, which is an important issue in the presence of a two-photon interaction. It is well known that the two-photon Dicke Hamiltonian undergoes a spectral instability in the ultrastrong coupling regime, when discrete energy levels collapse into a continuous band [58–60]. This dynamical property is preserved in the presence of bosonic field decay [18]. For the present case (including qubit dissipation) an "instable phase" (I) has been revealed by a study of stable fixed points [61]. However, considering the explicit time evolution, we generally find here a stable, albeit complex, dynamics. From this perspective, our study provides a precise characterization of the I-phase of Ref. [61].

The paper is organized as follows. In Sec. II, we describe the open two-photon Dicke model and explore its phase diagram in the mean-filed approximation, only considering stable fixed points. In Sec. III, we investigate the long-time nonlinear dynamics and find three distinct routes to chaos, depending on the qubit frequency: (1) period doubling; (2) intermittency; and (3) quasi-periodicity; In Sec. IV, we present the overall phase diagram, involving stable fixed points as well as chaos-related nonlinear dynamics. A comparison of our results with previous relevant research can also be found. Finally, we provide a summary of our findings in Sec. V.

II. THE MODEL

We consider a two-photon Dicke model described by the Hamiltonian [61]

$$\hat{H} = \omega_0 \hat{a}^\dagger \hat{a} + \frac{\omega_q}{2} \sum_{j=1}^{N} \hat{\sigma}_z^{(j)} + \frac{g}{\sqrt{N}} \sum_{j=1}^{N} \hat{\sigma}_x^{(j)} (\hat{a}^2 + \hat{a}^{\dagger 2}), \quad (1)$$

where $\hat{a}$ ($\hat{a}^\dagger$) is the annihilation (creation) operator of a bosonic field of frequency ω_0 and $\vec{\hat{\sigma}}^{(j)}$ are the Pauli operators of N qubits. The qubits have a uniform transition frequency ω_q and coupling strength g with the bosonic mode. As a consequence, Eq. (1) can be rewritten in terms of collective angular momentum operators $\vec{\hat{J}} = \frac{1}{2} \sum_{j=1}^{N} \vec{\hat{\sigma}}^{(j)}$ as follows:

$$\hat{H} = \omega_0 \hat{a}^\dagger \hat{a} + \omega_q \hat{J}_z + \frac{2g}{\sqrt{N}} \hat{X} \hat{J}_x. \quad (2)$$

Here, we have also defined $\hat{X} = \hat{a}^2 + \hat{a}^{\dagger 2}$ and $\hat{Y} = i(\hat{a}^2 - \hat{a}^{\dagger 2})$. The two-photon Dicke Hamiltonian is invariant under the generalized parity operator $\hat{\Pi} = (-1)^N \bigotimes_{j=1}^{N} \hat{\sigma}_z^{(j)} e^{i\pi \hat{a}^\dagger \hat{a}/2}$ [58], leading to

$$\hat{a} \to i\hat{a}, \quad \hat{\sigma}_{x,y} \to -\hat{\sigma}_{x,y}. \quad (3)$$

As a result, the system features a fourfold symmetry.

The two-photon Dicke Hamiltonian is well known for its spectral properties, with the discrete eigenenergy levels collapsing into a continuous band in the ultrastrong coupling regime [58–60]. Cavity field dissipation alone cannot eliminate this instability, as a diverging photon number is obtained when approaching the corresponding localized phase [18]. Before this instability, a superradiant-like phase transition takes place, in which the collective pseudospin attains a macroscopic mean value and the bosonic field is driven to a squeezed state [47,48,62]. As we will see, however, the properties of the model depend sensitively on the dissipative environment. In this work, we describe the system evolution with the standard master equation ($\hbar = 1$):

$$\dot{\hat{\rho}} = -i[\hat{H}, \hat{\rho}] + \kappa \mathcal{D}[\hat{a}]\hat{\rho} + \sum_{j=1}^{N} \left(\Gamma_\downarrow \mathcal{D}[\hat{\sigma}_-^{(j)}]\hat{\rho} + \Gamma_\phi \mathcal{D}\big[\hat{\sigma}_z^{(j)}\big]\hat{\rho} \right), \quad (4)$$

where the Lindblad superoperators are defined as $\mathcal{D}[\hat{A}]\hat{\rho} = 2\hat{A}\rho\hat{A}^\dagger - \hat{A}^\dagger\hat{A}\rho - \rho\hat{A}^\dagger\hat{A}$. As in Ref. [61], we include all three dissipation channels which naturally appear in the system: photon loss (κ), individual qubit decay ($\Gamma_\downarrow$), and individual qubit dephasing (Γ_ϕ). The Lindblad master equation is left unchanged by the transformation in Eq. (3) [i.e., $\hat{\Pi}^\dagger \hat{\rho} \hat{\Pi}$ is also a solution of Eq. (4)], thus retains the fourfold symmetry of the model.

In the following, we will focus on the limit of large N and consider coupling strengths comparable to the bosonic-field frequency, when the spin degrees of freedom acquire macroscopic populations. This justifies applying the mean-field approximation to the system's dynamics. Decoupling cavity-qubit correlations as $\langle \hat{C}\hat{Q} \rangle = \langle \hat{C} \rangle \langle \hat{Q} \rangle$, the following equations of motion are obtained:

$$\frac{d\langle \hat{X} \rangle}{dt} = -2\kappa \langle \hat{X} \rangle - 2\omega_0 \langle \hat{Y} \rangle, \quad (5)$$

$$\frac{d\langle \hat{Y} \rangle}{dt} = -2\kappa \langle \hat{Y} \rangle + 2\omega_0 \langle \hat{X} \rangle + 4g\sqrt{N} s_x (2\langle \hat{a}^\dagger \hat{a} \rangle + 1), \quad (6)$$

$$\frac{d\langle \hat{a}^\dagger \hat{a} \rangle}{dt} = -2\kappa \langle \hat{a}^\dagger \hat{a} \rangle + 2g\sqrt{N} s_x \langle \hat{Y} \rangle, \quad (7)$$

$$\frac{ds_x}{dt} = -\omega_q s_y - 2\Gamma' s_x, \tag{8}$$

$$\frac{ds_y}{dt} = \omega_q s_x - \frac{2g}{\sqrt{N}} s_z \langle \hat{X} \rangle - 2\Gamma' s_y, \tag{9}$$

$$\frac{ds_z}{dt} = \frac{2g}{\sqrt{N}} \langle \hat{X} \rangle s_y - 2\Gamma_\downarrow (s_z + 1), \tag{10}$$

where we rescaled the expectation values of the spin operators as $\vec{s} = \langle 2\vec{J} \rangle / N$ and defined $\Gamma' = 2\Gamma_\phi + \Gamma_\downarrow/2$. Due to the presence of qubit dissipation, the collective spin evolution will not be restricted to the unit sphere, giving a six-dimensional phase space (instead of the five-dimensional phase space of Ref. [18]).

As a first step of our investigation we focus on the stationary states, whose stability can be established from the Jacobian matrix and the Routh-Hurwitz criteria [1,63]. As expected, the system presents a phase transition from the normal phase (NP) to the superradiant phase (SP). The normal phase fixed point is [61]

$$\text{NP}: \quad s_z = -1, \langle \hat{a}^\dagger \hat{a} \rangle = 0, \tag{11}$$

and is stable for [61]

$$g < g_{t1} = \sqrt{\frac{(\kappa^2 + \omega_0^2)(\omega_q^2 + 4\Gamma'^2)}{4\omega_0 \omega_q}}. \tag{12}$$

The above results, and in particular Eq. (11), are only strictly valid within the mean-field approximation. In the limit of large N, the exact expectation values of the spin operators have deviations from $s_z = -1$ much smaller than 1. As we will see, the photon states acquires a macroscopic population of order N in the superradiant phase [see Eq. (13), where $\beta \propto 1/N$] and in the course of the dynamical evolution (see Fig. 3, where $\bar{n}_c = \langle \hat{a}^\dagger \hat{a} \rangle / N$). Thus, more precisely, the mean-field solution NP actually implies $\langle \hat{a}^\dagger \hat{a} \rangle \ll N$, rather than zero photons.

We also note that, in most literature, a $1/N$ scaling of the interaction is adopted in the two-photon Dicke Hamiltonian, i.e., the coupling strength is written as g/N [47,48,50,58,62]. However, from the point of view of the normal state instability, it is quite interesting to consider the alternative scaling $1/\sqrt{N}$, which we have used in Eq. (1). With this choice, as seen in the phase diagrams of Fig. 1 (white solid curves), there is a well-defined phase boundary independent of N [61]. If $1/N$ scaling were adopted in Eq. (1), the stability boundary would differ by a factor $\sqrt{N}$ in g_{t1}, giving a critical line which depends on qubit number. Considering the thermodynamic limit $N \to \infty$ at fixed g, the normal state would always be stable, as the critical line will shift right with increasing N. Therefore, in the following, we will restrict ourselves to the type of thermodynamic limit implied by Eq. (1), when the nontrivial instability of the normal phase remains independent of N.

The second type of fixed point is a superradiant state with excited spins ($s_z > -1$) and a nonzero photon number:

$$\text{SP}: \quad s_z = -\frac{1+\beta}{2} + \sqrt{\left(\frac{1+\beta}{2}\right)^2 - \beta \frac{g_{t1}^2}{g^2}},$$

$$\langle \hat{a}^\dagger \hat{a} \rangle = \frac{1}{2\beta}(s_z + 1), \tag{13}$$

where $\beta = \omega_0 \Gamma' / (N \omega_q \Gamma_\downarrow)$. As the system has a fourfold symmetry, the SP fixed points of Eq. (13) appear in pairs, distinguished by the values of $\pm\langle \hat{X} \rangle, \pm\langle \hat{Y} \rangle, \pm s_{x,y}$. In the parameter range of Fig. 1, the SP states are stable when $g_{t1} < g < g_{t2}$. g_{t2} is obtained numerically and plotted by the red dashed line in the figure. SP states also appear at large coupling strength, beyond the parameter range considered in this work [61]. As seen in Fig. 1, the SP phase shrinks with increasing qubit number.

The phase diagram for stable fixed points in Figs. 1(a) and 1(b) is plotted under small qubit dissipation and isotropic couplings. Phase NP (SP) indicates where the fixed point NP (SP) is stable. Phase I denotes the absence of a stable fixed point. More details on how the phase diagram changes with different system parameters can be found in Ref. [61], which investigates stationary dynamics of the two-photon Dicke model by the mean-field decoupling approximation. Considering the

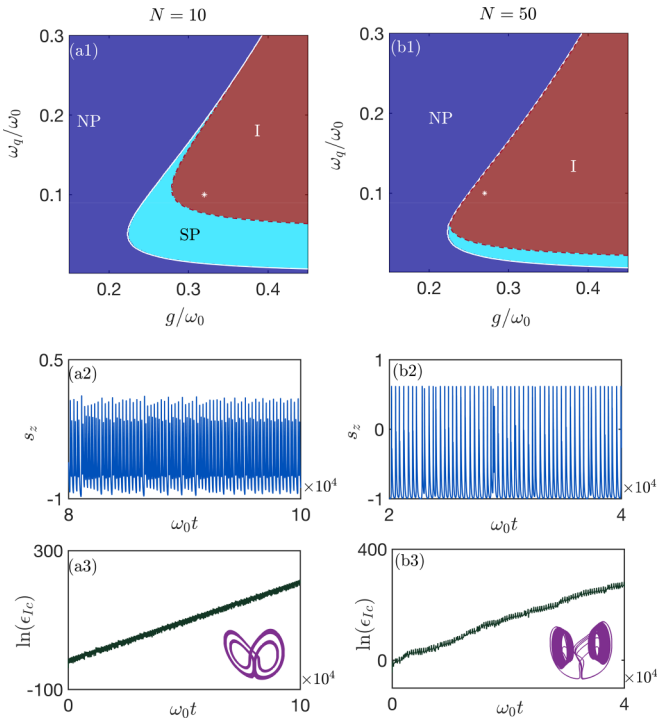

FIG. 1. (a1 and a2) Phase diagrams of stable fixed points for different N. The dark blue area represents the NP; the light blue area represents the SP, and the red area represents the phase without any stable fixed point (I). Critical point g_{t1} (white line) separates NP from other phases. g_{t2} (red dashed line) is the boundary of SP and phase I, which is obtained numerically. (a2 and a3) Chaotic motion in phase I for $N = 10$, $\omega_q/\omega_0 = 0.1$, $g/\omega_0 = 0.32$. (b2 and b3) Chaotic motion in phase I for $N = 50$, $\omega_q/\omega_0 = 0.1$, $g/\omega_0 = 0.27$. Insets: corresponding qubit trajectories in phase space. The other parameters are $\kappa/\omega_0 = 1$ and $\Gamma_\downarrow/\omega_0 = \Gamma_\phi/\omega_0 = 0.01$.

effects of both qubit and cavity dissipation, Ref. [61] indicates that, at isotropic coupling, there is a threshold of qubit dissipation beyond which only SP and bistable phases exist; otherwise, the unstable phase I occupies a large part of the phase diagram. While that study is limited to stationary states, the unstable region conceals abundant nonlinear dynamics. As shown in Figs. 1(a2)–1(b3), both in small ($N = 10$) and large ($N = 50$) systems, we found chaotic motions in the unstable phase I. Furthermore, other chaos-related nonlinear behaviors will be described in detail below.

Figures 1(a) and 1(b) have a simple structure when compared to the phase diagram of the anisotropic two-photon Dicke model [18], which considers unbalanced rotating and counterrotating coupling. Taking only cavity decay into account, the system displays a localized phase U_0 reflecting the spectral collapse of the closed-system Hamiltonian. In this U_0 phase, the system tends to evolve towards the poles of the Bloch sphere with a diverging photon number. At the same time, various coexistence phases lead to complex phase diagrams, which depend on initial conditions. The localized phase and various coexistence phases are absent in Fig. 1, which reflects the role of qubit dissipation in the stabilization of the two-photon Dicke model. Further, in Ref. [18], the anisotropic parameter λ plays an important role in the nonlinear behaviors since chaos is only found above a pole-flip transition: $\lambda > \lambda_t > 1$.

As an extension of the above studies, the current work is implemented with the isotropic condition $\lambda = 1$ and will focus on the nonlinear dynamics in the unstable phase. Small qubit decay is clearly more advantageous for our simulation, which will provide a large area of unstable phase. $\Gamma_\downarrow = \Gamma_\phi = 0.01\omega_0$ are adopted in Figs. 1(a) and 1(b), and will also be used throughout this work. Before presenting the main results, we note that system dynamics are inevitably influenced by qubit number, just as the above-mentioned studies. Though the cavity field does not exhibit a well-defined classical occupation in the SP phase, mean-field treatment is nevertheless applicable to the given system since the atomic field has a macroscopic population [18]. The mean-field approximation has little effect on I phase, which exhibits a macroscopic oscillation in the evolution of $\bar{n}_c(t) = \langle \hat{a}^\dagger \hat{a} \rangle(t)/N$. As shown in the insets of Figs. 4(a3) and 4(b3), the photon field oscillation is about $0 < \bar{n}_c(t) < 8$ with small qubit number $N = 10$. Large fluctuations of photon field also pose higher requirements for computing accurately the dynamics, especially in larger systems. Since chaos can be found in both small and large systems (it is actually easier to discover in large systems), we adopt $N = 10$ throughout our calculation to mitigate numerical difficulties caused by large qubit numbers.

III. ROUTES TO CHAOS

Even though there is no stable fixed point in phase I, it is more complicated than it looks: we found various types of nonlinear dynamics in this phase, such as periodic, quasi-periodic, and chaotic motion. Generally, chaos can appear in a nonlinear three- (or higher) dimensional deterministic system via local bifurcation. In the discussed two-photon Dicke model, altering qubit frequency ω_q allows chaos to manifest in three distinct ways. In the following, we present a detailed analysis of the bifurcation processes of how the system enters into the chaotic regime by (1) period-doubling bifurcation, (2) intermittency, and (3) quasi-periodicity.

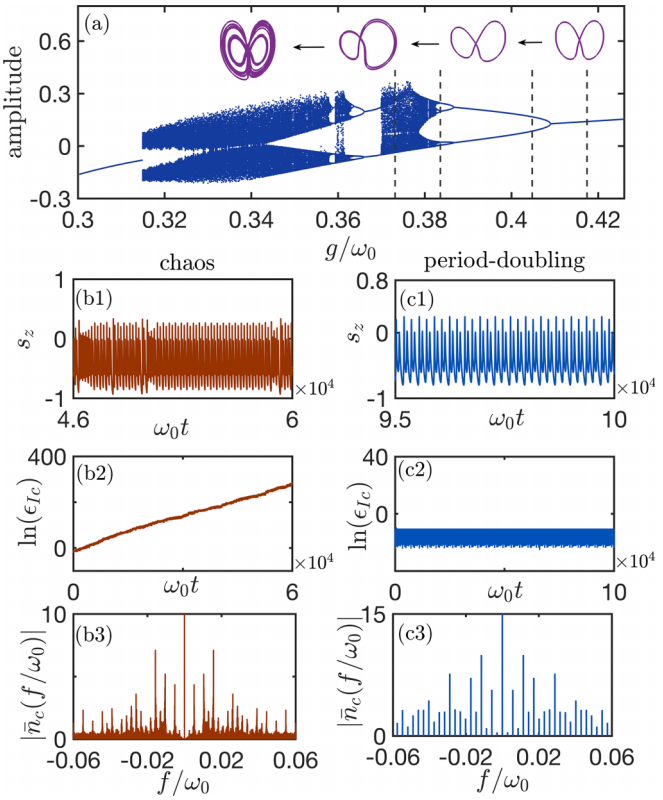

FIG. 2. Evolution from periodic to chaotic motion through period-doubling bifurcation. (a) Bifurcation phase diagram for $\omega_q/\omega_0 = 0.1$ which plots the oscillation amplitudes of $s_z(t) = 2\langle \hat{J}_z \rangle(t)/N$. The insets (from right to left) present the bifurcation of qubit trajectories from the symmetry limit cycle, unsymmetric limit cycle, via period doubling to chaos. The dashed black lines indicate the values of parameters. (b1–b3) Chaotic dynamics ($g/\omega_0 = 0.384$) by qubit evolution $s_z(t)$, perturbations of cavity field $\ln(\epsilon_{I_c})$, and power spectrum density of photon field, respectively. (c1–c3) Evolution of period doubling ($g/\omega_0 = 0.373$). Other parameters are the same as Fig. 1.

A. Period-doubling bifurcation

For a small value of qubit frequency, we found period-doubling bifurcation and cascade leading to chaos. Using the bifurcation diagram in Fig. 2(a), we illustrated in detail how a limit cycle transformed into a chaotic attractor. It is obviously seen that oscillations give a single amplitude at large g, while gradually bifurcating to 2^n ($n = 1, 2, 3, \ldots$) amplitudes as g decreases. As a typical route to chaos, period-doubling bifurcation has been observed in the anisotropic two-photon Dicke model. Differently, the bifurcation of the periodic orbit here begins with a symmetric-broken limit cycle. For large coupling, qubit trajectory in phase space first exhibits a limit cycle with two symmetric loops, displaying one amplitude in the bifurcation diagram, which consists of the amplitudes of $s_z(t)$. To simplify the observation of bifurcation, we hide the axes of $s_{x,y,z}$ in the insets of qubit trajectories. The two loops become unsymmetrical with the decreasing coupling strength,

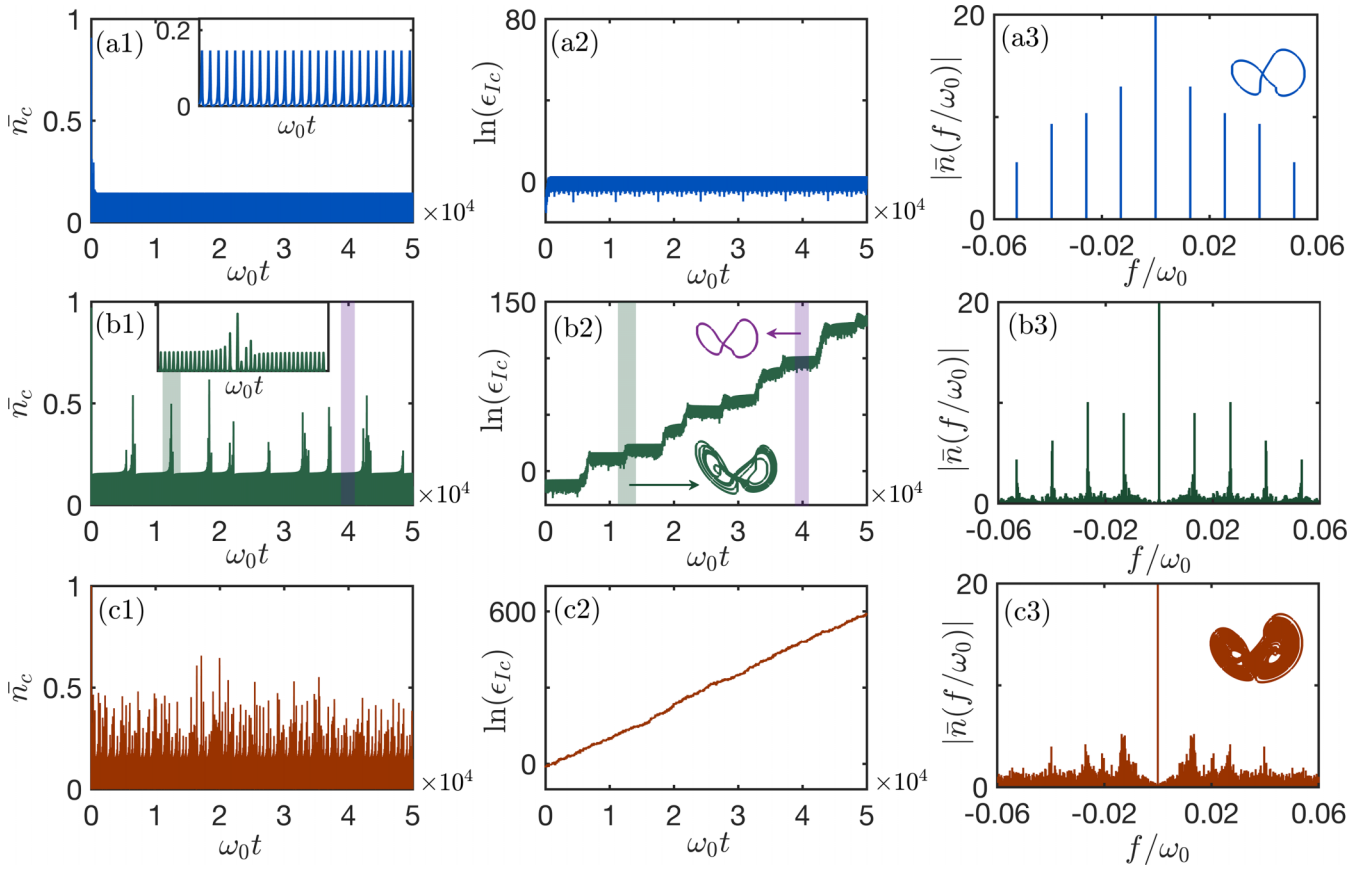

FIG. 3. Evolution from periodic to fully chaotic motion via IC. By plotting the time evolution of photon field $\bar{n}_c = \langle \hat{a}^\dagger \hat{a} \rangle / N$, perturbation, and photon field spectrum in the columns from left to right, we present periodic evolution ($g/\omega_0 = 0.3763$), intermittent chaos ($g/\omega_0 = 0.3795$), and fully chaotic dynamics ($g/\omega_0 = 0.3826$) in (a)–(c), respectively. For better insight, we enlarge part of intermittency dynamics (green shaded) in the inset of (b1). Correspondingly, insets in (b2) display system trajectories of chaotic (green) and periodic sectors (purple) in IC. A medium value of qubit frequency $\omega_q/\omega_0 = 0.15$ is used in the calculation. Other parameters are the same as Fig. 1.

presenting two amplitudes. When the coupling strength decreases further, it splits into a new one with four loops, resulting in quadruple amplitudes in the phase diagram. The corresponding dynamics are depicted in Fig. 2(c), where the system evolution shows four amplitudes with fourth periods of the original simple cyclic motion. Dynamics in a regular orbit provides a flat form in the evolution of cavity field perturbation $\ln(\epsilon_{Ic})$, the slope of which determines the value of the Lyapunov exponent (LE). Several discrete peaks can be found in the power spectral density (PSD) of photon number $\bar{n}_c = \langle \hat{a}^\dagger \hat{a} \rangle / N$. They are equally spaced in the figure, indicating that the frequency ratios are rational. By further decreasing g, cascading of bifurcation occurs. The system finally enters the chaotic regime with infinite amplitudes. Figure 2(b) depicts chaotic dynamics, which presents a random oscillation with variable amplitude and a continuous spectrum. In phase space, even infinitesimally nearby trajectories will rapidly deviate from one another, leading to an exponential growth of the perturbation and a positive LE.

B. Intermittency

We discovered that chaos can emerge through intermittent motion when system settings are changed for the medium value of qubit frequency. Intermittency describes dynamics switching between different types of oscillations under fixed control parameters. The switching appears to occur randomly, usually between regular and chaotic behaviors [2,64]. The detailed process of how chaos appears via intermittent chaos (IC) is exemplified in Fig. 3, where $\omega_q/\omega_0 = 0.15$ is adopted.

For small coupling strength, the system evolves on a periodic orbit that is formed by the fixed point SP via Hopf bifurcation. Stable oscillation with constant amplitude is shown in Fig. 3(a). As stated in the previous section, periodic dynamics offer a flat shape in the evolution of perturbation $\ln(\epsilon_{Ic})$ and equidistant discrete peaks in the power spectrum. With increasing coupling strength, occasional bursts of irregular motion in periodic dominant evolution occur. It can be seen from Fig. 3(b) that, along with time, system behavior switches between period and chaos for constant system parameters, giving rise to a ladder form in the evolution of $\ln(\epsilon_{Ic})$. In Fig. 3(b2), short-lived chaos generates the leap part, presenting a strange attractor in phase space (inset plotted by the green line). The flat part corresponds to periodic oscillation, which produces a limit cycle (inset plot by the purple line). During the evolution, system trajectory vacillates between periodic orbits and chaotic attractors. This particular intermittence feature is also demonstrated clearly in the PSD of the cavity field, which distinguishes several equally spaced discrete peaks from numerous small sidebands. Occasional

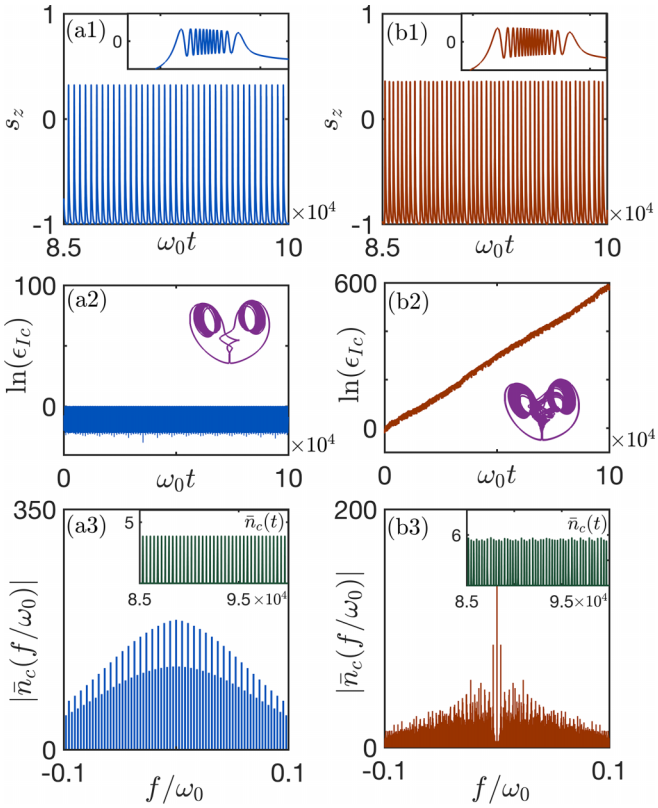

FIG. 4. Evolution from quasi-periodic (left panel: $g/\omega_0 = 0.3716$) to chaotic motion (right panel: $g/\omega_0 = 0.3795$) for large qubit frequency $\omega_q/\omega_0 = 0.25$. The inset in (a1) and (b1) is the blowup of a random prominent peak of $s_z(t)$. In the discrete spectrum (a3), the main frequencies are at integer multiples of $f_1 = 5.3 \times 10^{-3}\omega_0$, and the distance between auxiliary frequency peaks is $f_2 = 2.6 \times 10^{-4}\omega_0$. Inset in (b2): chaotic attractor. Insets in (a3) and (b3): evolution of cavity field $\bar{n}_c = \langle \hat{a}^\dagger \hat{a} \rangle / N$. Other parameters are the same as in Fig. 1.

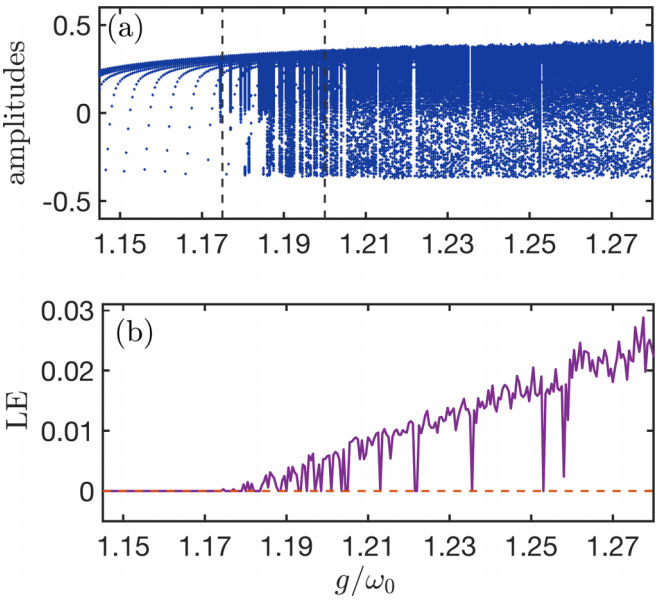

FIG. 5. (a) Amplitude statistics of qubit oscillation $s_z(t)$ during quasi-periodicity to chaos. The dashed lines mark the quasi-periodic and chaotic dynamics presented in Fig. 4. (b) Corresponding values of the LE. The dashed line denotes the zero value. Other parameters are as in Fig. 4.

chaotic motion becomes more frequent and lasts longer with further increasing coupling strength. Eventually, the system enters a fully chaotic phase, displaying irregular oscillation, a sloped version of $\ln(\epsilon_{Ic})(t)$, and a continuous spectrum, see Fig. 3(c). In comparison with periodic and intermittent spectra, no dominant frequency can be recognized from the chaotic continuous spectrum.

C. Quasi-periodicity

For large qubit frequency, we found that chaos emerges by way of quasi-periodicity. As can be seen from Fig. 4(a1), the qubit behaves deceptively with periodic oscillation when the coupling strength is small. Actually, the trajectory never repeats itself exactly. Each prominent peak of the quasi-periodicity includes several additional minor oscillations, presenting a number of amplitudes. Physically, the spins in our system can be regarded as an oscillator with a nonlinear coupling to another harmonic oscillator—the bosonic field. The interaction of the two nonlinear oscillators introduces additional frequencies. If the ratio of the frequencies is rational, system dynamics show periodic motion, as we have presented in the previous sections. On the contrary, the system exhibits quasi-periodicity if the ratio is irrational [2,56].

In the quasi-periodic scenario, the system trajectory will drift slightly with the change of initial conditions, resulting in a small distance from the original trajectory that will not diverge with time. On the one hand, it produces a flat shape in the evolution of $\ln(\epsilon_{Ic})$, i.e., zero LE. On the other hand, the long time trajectory will cover the surface of a tour in phase space. As can be seen from the inset in Fig. 4(a2), the trajectory that corresponds to the additional minor oscillations is crammed into two ring surfaces. Under the competition of the two modes, quasi-periodicity creates a distinct power spectrum with periodic oscillation, see Fig. 4(a3). Though it consists of discrete peaks, the frequencies are not evenly distributed. The dominant peaks are situated at $0, \pm f_1, \pm 2f_1, \ldots$, with auxiliary peaks spaced at f_2 bunched around them. With increasing coupling strength, each oscillation comprises a growing number of amplitudes. The trajectories from the two tours spread and interweave, finally leading to chaotic motion, seen in Fig. 4(b). Correspondingly, positive LE and continuous spectrum also can be seen in the picture.

Similar to the bifurcation diagram in Fig. 2, we record the amplitudes of $s_z(t)$ during the appearance of chaos through quasi-periodicity. As shown in Fig. 5(a), both quasi-periodic and chaotic oscillation show a larger number of peaks, while the former can be counted. When the dynamic of the system gets chaotic, an overwhelming number of amplitudes arise in a narrow band of g, producing a dense concentration of points in the picture. The variation of the Lyapunov exponent with coupling strength is shown in Fig. 5(b), which is in good agreement with the amplitude statistics graph. LE is close to zero in the domain of finite amplitudes, corresponding to

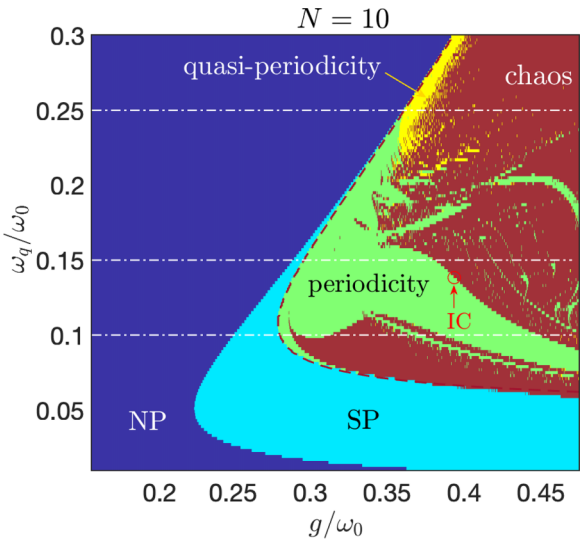

FIG. 6. Overall phase diagram. It contains stable phases [NP (dark blue) and SP (light blue)] and oscillatory phases [periodic (green), quasi-periodic (yellow), intermittent chaos (red spots), and full chaos (brown)]. The dashed-dotted lines mark the values of qubit frequencies that we have used in previous figures. The red dashed line is the critical boundary g_{t2}. Other parameters are the same as in Fig. 1.

quasi-periodic oscillations. Positive LE, as reflected by infinite amplitudes, provides evidence for the existence of chaos.

IV. OVERALL PHASE DIAGRAM

The emergence of chaos in various ways results from the nonlinear interaction between the spin and cavity field. The inclusion of qubit dissipation enables us to treat it as a spin whose dynamics will not be constrained on the Bloch sphere anymore. Including stable fixed points and chaotic dynamics, we provide in Fig. 6 the overall phase diagram as function of coupling strength g and qubit frequency ω_q. The stable phases NP and SP are indicated by dark and light blue areas in the figure. The unstable phase in Fig. 1 now is replaced by periodicity (green), quasi-periodicity (yellow), intermittent chaos (red), and full chaotic (brown) phases. When calculating the phase diagram, it is useful to distinguish periodic motion and quasi-periodicity from intermittency and chaos using the Lyapunov exponent, where regular oscillations yield zero values and chaotic dynamics produce positive values. Consequently, we need to differentiate quasi-periodicity from the period. Both of them have discrete spectra and zero LE. We can recognize quasi-periodicity by its nonrepetitive and irregular time evolution. When compared to periodic oscillation, significantly increased amplitudes could be discovered in quasi-periodicity during the same time interval. Moreover, the amplitudes generated by quasi-periodicity will change with oscillation time and sampling frequency. Also, we can identify quasi-periodicity by the power spectrum, which shows an irrational ratio of frequencies. Then, we can separate intermittency and full chaos through the ladder form of $\ln(\epsilon_{Ic})(t)$.

As we can see from the figure, the system evolves on a periodic orbit produced by fixed-point SP via Hopf bifurcation when the coupling strength is slightly larger than g_{t2}. Due to the competition between the spin and bosonic modes, an additional frequency may arise as the coupling strength increases. The dashed-dotted lines indicate the position of the three typical qubit frequencies that have been used in Figs. 2–5. For small qubit frequency, which is represented by $\omega_q/\omega_0 = 0.1$ (bottom line), one mode is locked by another one under strong coupling, leading to period-doubling dynamics over a finite control parameter regime. The output light will display intense bursts or pulses, which is a very popular way of generating frequency comb. By properly adjusting system parameters, the two modes exhibit balanced influences on the system, which gives rise to intermittent chaos. The parameters we used in Fig. 3, which show the process of intermittent chaos to full chaos, are chosen along the middle line $\omega_q/\omega_0 = 0.15$. IC is uncommon in our system; it only shows several spots in the picture. For large qubit frequency, the frequency induced by the two competition modes will show a slight deviation from the original frequency. Incommensurate frequencies lead to irregular oscillation and quasi-periodicity. Before approaching the quasi-periodic state, the system usually experiences a periodic phase that diminishes with increasing qubit frequency.

Now we can compare the dynamics of the current model to the anisotropic two-photon Dicke model that only considers cavity field dissipation [18]. Aside from the differences highlighted in the phase diagram of stable fixed points, see Sec. II, the present model also exhibits distinct nonlinear dynamics. In Ref. [18], chaos can only be found in an anisotropic model ($\lambda > \lambda_t > 1$), and appears through a cascade of period-doubling bifurcations. For a given set of parameters, multiple types of motion coexist in phase space, resulting in a phase diagram which depends on the system's initial state. The current work, which is implemented in the isotropic instance $\lambda = 1$, likewise shows the presence of chaos. However, besides arising from a cascade of period-doubling bifurcations, chaos can occur via intermittency and quasi-periodicity by adjusting the qubit frequency, creating a complex phase diagram. Since we do not find the coexistence of different motions, the phase diagram will not be influenced by the system's initial state. Other chaos-related dynamics, such as the occurrence of windows of periodicity and collision of chaotic attractors, can also be discovered in the current model but are not discussed here in detail.

V. CONCLUSION

In conclusion, we investigated the semiclassical nonlinear dynamics of the two-photon Dicke model showing that, in the presence of qubit dissipation, three distinct routes to chaos can appear. Qubit decay and dephasing help to stabilize the system, as we do not find here a localized phase (reflecting the spectral collapse of the Hamiltonian) or phase coexistence [18]. Besides normal and superradiant phases, a variety of chaos-related phenomena survives in a large region of parameters, even restricting ourselves to balanced co- and counterrotating couplings. More interestingly, through the manipulation of qubit frequency, chaos can appear in three distinct ways: a period-doubling route for small ω_q, intermittent motion for a moderate value of ω_q,

and quasi-periodic oscillations for large ω_q. We provide a comprehensive illustration of the transitions using bifurcation diagrams and a global chaotic phase diagram. Comparisons of our findings to prior research in the field also have been made.

It might be possible to realize the dissipative two-photon Dicke model in driven systems such as trapped ion chains and quantum superconducting circuits, which can eliminate undesirable effects caused by ultrastrong coupling in loss-dominated systems [39,45,58,65,66]. Under effective implementations of the model, coupling strength can be comparable to (or even larger than) the bosonic and atomic (effective) frequencies, as well as considered decoherence and dissipation processes. The dissipation channels can be tailored in strongly driven atomic cloud or quantum simulation systems using bath-engineering approaches [67–71].

The present discussion considers the semiclassical limit of the collective spin variables, which at large N becomes an accurate description of one- and two-photon Dicke models (see, e.g., Refs. [18,27,72] for explicit comparisons to the exact quantum solution). Still, it would be of great interest to investigate how these nonlinear phenomena manifest themselves in fully quantum treatments [73–75]. Studies have shown that signatures of dissipative quantum chaos can be detected by the Liouvillian superoperator, whose spectrum shows unique statistical properties [76–83]. Furthermore, quantum Lyapunov exponents have been computed in the closed Dicke model from the out-of-time-ordered correlator (OTOC) [52]. The anisotropic coupling may also be included in the present dissipative Dicke model, which would likely result in more complicated dynamics and phase diagrams. Our investigation into the nonlinear dynamics of this dissipative quantum system may stimulate further research on quantum chaos, the findings of which may be applicable to quantum on-chip devices and communications.

ACKNOWLEDGMENTS

We gratefully acknowledge R. Fazio for his helpful discussions. S.C. acknowledges support from the Innovation Program for Quantum Science and Technology (Grant No. 2021ZD0301602), the National Science Association Funds (Grant No. U2230402), and the National Natural Science Foundation of China (Grants No. 11974040 and No. 12150610464).

[1] S. H. Strogatz, *Nonlinear Dynamics and Chaos: With Applications to Physics, Biology, Chemistry, and Engineering* (CRC Press, Boca Raton, 2018).
[2] R. C. Hilborn *et al.*, *Chaos and Nonlinear Dynamics: An Introduction for Scientists and Engineers* (Oxford University, New York, 2000).
[3] J. Ma, C. You, L.-G. Si, H. Xiong, J. Li, X. Yang, and Y. Wu, Phys. Rev. A **90**, 043839 (2014).
[4] L. Bakemeier, A. Alvermann, and H. Fehske, Phys. Rev. Lett. **114**, 013601 (2015).
[5] M. Wang, X.-Y. Lü, J.-Y. Ma, H. Xiong, L.-G. Si, and Y. Wu, Sci. Rep. **6**, 22705 (2016).
[6] D. Navarro-Urrios, N. E. Capuj, M. F. Colombano, P. D. García, M. Sledzinska, F. Alzina, A. Griol, A. Martínez, and C. M. Sotomayor-Torres, Nat. Commun. **8**, 14965 (2017).
[7] G.-L. Zhu, C.-S. Hu, Y. Wu, and X.-Y. Lü, Fundam. Res. **3**, 63 (2023).
[8] T. Hula, K. Schultheiss, A. Buzdakov, L. Körber, M. Bejarano, L. Flacke, L. Liensberger, M. Weiler, J. M. Shaw, H. T. Nembach *et al.*, Appl. Phys. Lett. **117**, 042404 (2020).
[9] Z.-X. Liu, C. You, B. Wang, H. Xiong, and Y. Wu, Opt. Lett. **44**, 507 (2019).
[10] B. Wang, X. Jia, X.-H. Lu, and H. Xiong, Phys. Rev. A **105**, 053705 (2022).
[11] W.-L. Xu, X.-F. Liu, Y. Sun, Y.-P. Gao, T.-J. Wang, and C. Wang, Phys. Rev. E **101**, 012205 (2020).
[12] K. Hepp and E. H. Lieb, Phys. Rev. A **8**, 2517 (1973).
[13] P. Kirton, M. M. Roses, J. Keeling, and E. G. Dalla Torre, Adv. Quantum Technol. **2**, 1800043 (2019).
[14] X.-H. Cheng, I. Arrazola, J. S. Pedernales, L. Lamata, X. Chen, and E. Solano, Phys. Rev. A **97**, 023624 (2018).
[15] S. Felicetti, D. Z. Rossatto, E. Rico, E. Solano, and P. Forn-Díaz, Phys. Rev. A **97**, 013851 (2018).
[16] K. C. Stitely, A. Giraldo, B. Krauskopf, and S. Parkins, Phys. Rev. Res. **2**, 033131 (2020).
[17] P. Kirton and J. Keeling, New J. Phys. **20**, 015009 (2018).
[18] J. Li, R. Fazio, and S. Chesi, New J. Phys. **24**, 083039 (2022).
[19] R. H. Dicke, Phys. Rev. **93**, 99 (1954).
[20] F. Dimer, B. Estienne, A. S. Parkins, and H. J. Carmichael, Phys. Rev. A **75**, 013804 (2007).
[21] M.-J. Hwang, R. Puebla, and M. B. Plenio, Phys. Rev. Lett. **115**, 180404 (2015).
[22] E. G. Dalla Torre, Y. Shchadilova, E. Y. Wilner, M. D. Lukin, and E. Demler, Phys. Rev. A **94**, 061802(R) (2016).
[23] J. Larson and E. K. Irish, J. Phys. A: Math. Theor. **50**, 174002 (2017).
[24] M. Fitzpatrick, N. M. Sundaresan, A. C. Y. Li, J. Koch, and A. A. Houck, Phys. Rev. X **7**, 011016 (2017).
[25] E. M. Kessler, G. Giedke, A. Imamoglu, S. F. Yelin, M. D. Lukin, and J. I. Cirac, Phys. Rev. A **86**, 012116 (2012).
[26] M. Liu, S. Chesi, Z.-J. Ying, X. Chen, H.-G. Luo, and H.-Q. Lin, Phys. Rev. Lett. **119**, 220601 (2017).
[27] P. Kirton and J. Keeling, Phys. Rev. Lett. **118**, 123602 (2017).
[28] M.-J. Hwang, P. Rabl, and M. B. Plenio, Phys. Rev. A **97**, 013825 (2018).
[29] J. Gelhausen, M. Buchhold, and P. Strack, Phys. Rev. A **95**, 063824 (2017).
[30] J. Gelhausen and M. Buchhold, Phys. Rev. A **97**, 023807 (2018).
[31] C. Emary and T. Brandes, Phys. Rev. E **67**, 066203 (2003).
[32] C. Emary and T. Brandes, Phys. Rev. Lett. **90**, 044101 (2003).
[33] X.-W. Hou and B. Hu, Phys. Rev. A **69**, 042110 (2004).
[34] N. Lambert, Y.-n. Chen, R. Johansson, and F. Nori, Phys. Rev. B **80**, 165308 (2009).
[35] P. Pérez-Fernández, A. Relaño, J. M. Arias, P. Cejnar, J. Dukelsky, and J. E. García-Ramos, Phys. Rev. E **83**, 046208 (2011).

[36] R. F. Bishop, N. J. Davidson, R. M. Quick, and D. M. van der Walt, Phys. Rev. A **54**, R4657 (1996).
[37] S. Ashhab and F. Nori, Phys. Rev. A **81**, 042311 (2010).
[38] R. Puebla, J. Casanova, and M. B. Plenio, New J. Phys. **18**, 113039 (2016).
[39] D. Lv, S. An, Z. Liu, J.-N. Zhang, J. S. Pedernales, L. Lamata, E. Solano, and K. Kim, Phys. Rev. X **8**, 021027 (2018).
[40] L. J. Zou, D. Marcos, S. Diehl, S. Putz, J. Schmiedmayer, J. Majer, and P. Rabl, Phys. Rev. Lett. **113**, 023603 (2014).
[41] F. Beaudoin, J. M. Gambetta, and A. Blais, Phys. Rev. A **84**, 043832 (2011).
[42] L. Lamata, Sci. Rep. **7**, 43768 (2017).
[43] F.-Y. Zhang, W.-B. Yan, and C.-P. Yang, Phys. Rev. A **98**, 042331 (2018).
[44] I. Travěnec, Phys. Rev. A **85**, 043805 (2012).
[45] R. Puebla, M.-J. Hwang, J. Casanova, and M. B. Plenio, Phys. Rev. A **95**, 063844 (2017).
[46] F. H. Maldonado-Villamizar, C. Huerta Alderete, and B. M. Rodríguez-Lara, Phys. Rev. A **100**, 013811 (2019).
[47] L. Garbe, I. L. Egusquiza, E. Solano, C. Ciuti, T. Coudreau, P. Milman, and S. Felicetti, Phys. Rev. A **95**, 053854 (2017).
[48] X.-Y. Chen and Y.-Y. Zhang, Phys. Rev. A **97**, 053821 (2018).
[49] Y.-F. Xie, L. Duan, and Q.-H. Chen, Phys. Rev. A **99**, 013809 (2019).
[50] S. Cui, F. Hébert, B. Grémaud, V. G. Rousseau, W. Guo, and G. G. Batrouni, Phys. Rev. A **100**, 033608 (2019).
[51] W. Buijsman, V. Gritsev, and R. Sprik, Phys. Rev. Lett. **118**, 080601 (2017).
[52] J. Chávez-Carlos, B. López-del-Carpio, M. A. Bastarrachea-Magnani, P. Stránský, S. Lerma-Hernández, L. F. Santos, and J. G. Hirsch, Phys. Rev. Lett. **122**, 024101 (2019).
[53] S. Wang, S. Chen, and J. Jing, Phys. Rev. E **100**, 022207 (2019).
[54] Q. Wang and M. Robnik, Phys. Rev. E **102**, 032212 (2020).
[55] A. Patra, B. L. Altshuler, and E. A. Yuzbashyan, Phys. Rev. A **99**, 033802 (2019).
[56] A. Patra, B. L. Altshuler, and E. A. Yuzbashyan, Phys. Rev. A **100**, 023418 (2019).
[57] S. Lerma-Hernández, D. Villaseñor, M. A. Bastarrachea-Magnani, E. J. Torres-Herrera, L. F. Santos, and J. G. Hirsch, Phys. Rev. E **100**, 012218 (2019).
[58] S. Felicetti, J. S. Pedernales, I. L. Egusquiza, G. Romero, L. Lamata, D. Braak, and E. Solano, Phys. Rev. A **92**, 033817 (2015).
[59] L. Duan, Y.-F. Xie, D. Braak, and Q.-H. Chen, J. Phys. A: Math. Theor. **49**, 464002 (2016).
[60] L. Cong, X.-M. Sun, M. Liu, Z.-J. Ying, and H.-G. Luo, Phys. Rev. A **99**, 013815 (2019).
[61] L. Garbe, P. Wade, F. Minganti, N. Shammah, S. Felicetti, and F. Nori, Sci. Rep. **10**, 13408 (2020).
[62] P. Banerjee, D. Sharma, and A. B. Bhattacherjee, Phys. Lett. A **446**, 128287 (2022).
[63] E. X. DeJesus and C. Kaufman, Phys. Rev. A **35**, 5288 (1987).
[64] D.-W. Zhang, C. You, and X.-Y. Lü, Phys. Rev. A **101**, 053851 (2020).
[65] S. Felicetti, M.-J. Hwang, and A. Le Boité, Phys. Rev. A **98**, 053859 (2018).
[66] D. De Bernardis, P. Pilar, T. Jaako, S. De Liberato, and P. Rabl, Phys. Rev. A **98**, 053819 (2018).
[67] J. F. Poyatos, J. I. Cirac, and P. Zoller, Phys. Rev. Lett. **77**, 4728 (1996).
[68] F. Verstraete, M. M. Wolf, and J. Ignacio Cirac, Nat. Phys. **5**, 633 (2009).
[69] K. Baumann, C. Guerlin, F. Brennecke, and T. Esslinger, Nature (London) **464**, 1301 (2010).
[70] N. Liu, J. Lian, J. Ma, L. Xiao, G. Chen, J. Q. Liang, and S. Jia, Phys. Rev. A **83**, 033601 (2011).
[71] M. Asjad and D. Vitali, J. Phys. B: At. Mol. Opt. Phys. **47**, 045502 (2014).
[72] N. Shammah, N. Lambert, F. Nori, and S. De Liberato, Phys. Rev. A **96**, 023863 (2017).
[73] S. Wimberger, *Nonlinear Dynamics and Quantum Chaos* (Springer, New York, 2014), Vol. 10.
[74] R. Grobe, F. Haake, and H.-J. Sommers, Phys. Rev. Lett. **61**, 1899 (1988).
[75] G. Akemann, M. Kieburg, A. Mielke, and T. Prosen, Phys. Rev. Lett. **123**, 254101 (2019).
[76] L. Sá, P. Ribeiro, and T. Prosen, Phys. Rev. X **10**, 021019 (2020).
[77] D. Huybrechts, F. Minganti, F. Nori, M. Wouters, and N. Shammah, Phys. Rev. B **101**, 214302 (2020).
[78] I. I. Arkhipov, A. Miranowicz, F. Minganti, and F. Nori, Phys. Rev. A **102**, 033715 (2020).
[79] J. Thingna and D. Manzano, Chaos **31**, 073114 (2021).
[80] F. Minganti, I. I. Arkhipov, A. Miranowicz, and F. Nori, Phys. Rev. Res. **3**, 043197 (2021).
[81] J. Li, T. Prosen, and A. Chan, Phys. Rev. Lett. **127**, 170602 (2021).
[82] I. Yusipov and M. Ivanchenko, Chaos **32**, 043106 (2022).
[83] S. Lange and C. Timm, Chaos **31**, 023101 (2021).